Sepsis-Induced Brain State Instability

Annu Kala
Charles University
Susan Leemburg
Charles University
Karel Jezek (karel.jezek@lfp.cuni.cz)
Charles University

Research Article

Keywords: Sepsis, Lipopolysacharide, EEG, Sleep, REM, NonREM

Posted Date: March 15th, 2022

DOI: https://doi.org/10.21203/rs.3.rs-1434896/v1

Abstract

Background

Sepsis-associated brain dysfunction (SABD) is a frequent severe complication of sepsis and the systemic inflammatory response syndrome. It is associated with high mortality and a majority of survivors suffer long-term neurological consequences. Sleep is commonly affected in sepsis and there is a strong correlation between its impairment and development of other complications or increased mortality in sepsis patients. Here, we investigate the effects of sepsis on brain activity patterns in order to better understand possible sources of sleep-wake disturbances associated with severe systemic inflammation.

Methods

We studied the effects of high LPS doses (10mg/kg) on oscillatory brain states in an acute rat model of sepsis under urethane anaesthesia, which maintains REM- and NREM sleep-like states. Twelve Long-Evans rats (6 LPS, 6 controls) were implanted with eight independently movable tetrodes in the dorsal hippocampus. Baseline LFP activity was recorded for 3 hours after saline injection, followed by another 3 hours after LPS or saline injection. REM and NREM were automatically classified based on LFP activity and quantified. Within- and between-state dynamics were analysed using a 2-D state space approach based on spectral power ratios. Aperiodic and periodic components of the power spectrum were quantified for each state. Blood serum samples and brains were collected for IL-1β quantification and histological verification of electrode placement.

Results

Soon after LPS injection we observed a robust fragmentation of both oscillatory states resulting in a three-fold increase in the number of state transitions that lasted for several hours, although the overall time spent in either state did not change. Analysis of power spectra showed opposing shifts in low frequency oscillations (1–9 Hz) in REM and NREM that resulted in increased similarity between both states in 2-D state space.

Conclusions

The observed increased spectral similarity between REM and NREM and increased instability within the states may point to a mechanism underlying the severe sleep fragmentation described both in sepsis patients and in SABD animal models.

Background

Sepsis, a state of dysregulated host response against an infection, affects around 30 million people each year and has 33% mortality [1, 2]. The brain is among the first impacted organ systems: up to 70% of sepsis patients suffer of Sepsis-associated brain dysfunction (SABD) early during the disease [4]. Out of those who survive, 20–25% experience post-sepsis syndrome, a long-term complex condition with increased risk of death and combining immunological, physical and psychological symptoms, severely reducing their quality of life [1, 5]. The latter might develop as sleep disturbances, psychiatric conditions or cognitive impairment, including mental confusion and concentration issues,

Within the brain, the hippocampus is one of the first areas to be affected by SABD. Given its role in learning and memory processing, alterations of hippocampal function during and after sepsis are of particular interest. Indeed, post-sepsis syndrome in septic shock survivors is often associated with long term memory impairments [6]. Sepsis resulted in decreased hippocampal volume, EEG abnormalities, and memory deficits, even in patients who showed no signs of the structural damage associated with SABD [7, 8]. In order to decrease sepsis-associated mortality and limit lasting nervous system damage, early detection of sepsis is critical. However, this is challenging due to the complex pathophysiology of the disease [9, 10].

Poor sleep quality during severe illness is common [11] and has been linked to the occurrence of delirium in sepsis patients [12]. Attempts to restore sleep quality using melatonin therapy in critically ill patients have proven to be helpful in improving the nocturnal sleep efficiency [13], but effects of these interventions on cognitive outcomes are yet to be studied. In addition to maintaining cognitive functions, sleep promotes survival and plays a vital role in maintaining immune system function. Poor sleep quality during severe illness may therefore lead to worse functional outcomes directly, but also by exacerbating immune dysfunction in the course of a disease.

Sepsis patients suffer from a variety of pathological brain activity patterns, including electrographic seizures and periodic discharges, as well as other changes in spectral and oscillatory activity. The rate of mortality and severe disability were directly proportional to the occurrence of electrographic seizures and periodic discharges, stressing the importance of early monitoring of brain activity [14].

Additionally, increased slow wave activity and decreased alpha power in the EEG have been associated with mortality in the ICU and predicted the occurrence of delirium in septic shock patients [15–17]. In a rat cecal-ligation-and-puncture model, sepsis led to acute sleep fragmentation and suppression of REM sleep, as well as an increase in the overall amount of dark phase NREM sleep [18]. Interestingly, slow wave activity was reduced during these periods of increased NREM sleep. A different study in anaesthetized rats using LPS-induced sepsis found reduced power in the 8–13 Hz alpha range, with no effects on delta power [19].

Under non-septic condition, immunological challenges such as low doses of LPS modulate sleep as well [20]. Low doses of LPS caused NREM fragmentation in rats and increased NREM slow wave activity while suppressing REM sleep [21]. Some of the observed effects of LPS on EEG spectra were similar to those of sleep deprivation, which might signify a common mechanism of EEG regulation in both

conditions. However, NREM fragmentation was specific to LPS administration, and typically does not occur during recovery after sleep deprivation [22, 23]. Similar effects of mild inflammation caused by LPS or Lipid A on NREM and REM sleep have been observed in rabbits [24]. Other studies in rats confirmed that low doses of LPS cause NREM discontinuity, but showed reduced NREM slow wave activity instead [25].

Apart from affecting overall sleep architecture and EEG, LPS has region-specific effects on brain oscillatory activity: Mamad et al. (2018) observed an acute slowing of hippocampal theta, with a concurrent increase in hippocampal delta frequency and power in awake rats. By contrast, prefrontal cortex showed no change in delta frequency, but exhibited reductions in theta frequencies and power [26]. The varying consequences of LPS on delta power in NREM could therefore be a result of species- or dose-specific effects, as well as time of injection and recorded brain region.

Despite being one of the first organs to be affected during sepsis, the role of and effects on the central nervous system are yet to be fully understood [27]. Electrophysiological changes of brain activity in sleep during acute sepsis could serve as a potential early biomarker of sepsis and related outcomes. Here, we aim to better understand the dynamics of REM-like and NREM-like states during severe acute systemic inflammation caused by a high dose of LPS (10 mg/kg). We used urethane anaesthesia as a model which mimics the unconscious state of sleep and produces sleep-like REM and NREM brain activity patterns [28]. Local field potentials from the CA3 region of the hippocampus were recorded in saline-injected and LPS-injected rats. LPS injection resulted in profound fragmentation of REM and NREM states. Additionally, spectral similarity between REM and NREM-like states was increased, particularly in lower frequencies (1–9 Hz). The observed spectral changes and instability may be a contributing factor to sepsis-related sleep disturbances and associated deficits in cognitive function.

Materials And Methods

Animals

Twelve adult Long-Evans rats weighing 400–500 grams were used. They were housed individually in transparent plexiglass cages and were kept in a 12:12 light/dark cycle with food and water *ad libitum*. Experiments were carried out during the light phase. All protocols were approved by the Ethical Committee of the Ministry of Education, Youth and Sports of the Czech Republic (approval no. MSMT-12084/2019) according to the Guide for the Care and Use of Laboratory Animals (Protection of Animals from Cruelty Law Act No. 246/92, Czech Republic.).

Experimental setup

To investigate the effects of acute systemic inflammation, two groups of rats were used (LPS and CTRL, N = 6 each, Fig. 1A). One hour after induction of urethane anesthesia, rats in both groups were injected with sterile saline (2ml/kg, i.p.). Then, baseline hippocampal activity was recorded for three hours. After this, rats in the LPS group were injected intraperitoneally with 10 mg/kg lipopolysaccharide and were

recorded for another three hours. Rats in the CTRL group received a second saline injection instead. After the second recording period, blood serum samples and brains were collected for IL-1β quantification and histological verification of electrode placement.

Electrode implantation surgery

Local field potentials were recorded from the rats implanted with eight independently movable tetrodes in the CA3 region of the hippocampus. Each tetrode consisted of four twisted 17-mm polyimide-coated platinum-iridium wires coated with platinum in order to reduce the impedance to 120–200 kΩ at 1 kHz.

Rats were anaesthetized using a mixture of ketamine (Narkamon, 100 mg/kg, i.p.) and xylazine (Rometar, 10 mg/kg, i.p.) and 1.5-2% isoflurane in O_2. They were fixed in a stereotaxic frame and body temperature was maintained 37°C using a heating pad. An incision was made in the scalp to expose the skull, after which a craniotomy was made over the dorsal hippocampus (3.8 mm AP, 3.2 mm lateral of bregma). After removal of the dura mater, the tetrode bundle was carefully lowered into the cortex. Individual tetrodes were slowly lowered into CA3 over the course of a 2-week recovery period. The hyperdrive was fixed to the skull using dental acrylic and stainless-steel screws. One screw, located above the frontal cortex, served as a reference. Rats were given carprofen (Rimadyl, 5 mg/kg, s.c.) and Marbofloxacin (Marbocyl, 5 mg/kg, s.c.) during recovery.

Recording procedure

Rats used were previously involved in behavioral experiments for 2–3 weeks after surgery. For the experiments described in this paper, rats were anesthetized for recording using urethane (1.5 g/kg, i.p., Sigma). An hour after urethane injection, hippocampal local field potentials were amplified using an Intan RHD2132 headstage amplifier, digitized and recorded using an OpenEphys recording system at a sampling rate of 2000 Hz [29].

Data processing and analysis

Signal processing

For vigilance state classification and later state-space analysis, a sliding window FFT analysis (2 s window, 1 s step) was performed on separately for all recorded channels using Welch's method in MATLAB 2014b (Hamming window, 50% overlap, 0.25 Hz resolution), yielding 1 epoch per second. Then, spectral ratios were calculated for overall power in two overlapping frequency ranges for each time window. Ratio 1 was calculated as R1 = (1–2 Hz)/(1–9 Hz) and Ratio 2 was calculated as R2 = (1–15 Hz)/(1–45 Hz). Frequency ranges were chosen based on literature and on the approximate frequencies of delta and theta peaks in our recorded baseline spectra [30, 31]. Normalized signal amplitude was calculated using the same sliding window approach, where mean absolute signal amplitude was calculated for each window and normalized to mean absolute signal amplitude for the entire recording. The resulting power and amplitude time series for all channels were then combined into a single time series per rat for each of these variables using PCA. The first principal component was used for further

analyses. Epochs that contained artifacts were excluded from further analysis (0.18 ± 0.06% of recording time). State labels for these epochs were set to be identical to the preceding, artifact-free epoch prior to smoothing.

Vigilance state classification and episode detection

Brain activity under urethane anaesthesia showed two distinct alternating states: a NREM-like state that was dominated by low frequency, high-amplitude waves, and a REM-like state with faster activity and a lower signal amplitude. Epochs were automatically classified as belonging to one of these states based on the calculated principal component values for R1, R2, and amplitude using k-means clustering. Inclusion of the amplitude parameter in the clustering procedure ensured reliable state identification, even when spectral ratios were affected by experimental treatment.

After initial clustering, ultra-short periods of NREM-like or REM-like activity were removed: a state transition was only considered if the first epoch of the new state was followed by at least 3 more epochs of the same state. Otherwise, the epoch was labelled as belonging to the preceding state. This ensured that any unrealistically short, artefactual state changes caused by normal within-state signal variability were removed.

NREM-like and REM-like episodes were calculated as periods of each state that were at least 10 epochs long, and were followed by at least 10 epochs of the other state. Short episodes were considered as 20–120 s long, whereas episodes of 600 s or more were considered long. Epoch-to-epoch transition probability was calculated based on the percentage of epoch that was followed by the same or a different state. Episode transitions were characterized by fitting a logistic curve using MATLAB's fit function with the following equation $f(x) = \text{offset} + (\text{range} / (1 + e^{-\text{slope}*x}))$. Curves were fit to a 30-s period of LFP trace centered on the episode state transition after smoothing using a 5-s window moving average.

State-space analysis

Inflammation-related spectral changes were analysed in a 2-dimensional state-space based on R1 and R2. This type of analysis may reveal within- and between state dynamics that are not captured using less sensitive single-band approaches [30, 31]. Cluster positions were defined using the median pc1R1 and pc1R2 values for each state.

Within-state stability was analyzed using state-space velocity. Velocity was defined as the Euclidian distance between two subsequent epochs. As such, overall velocity was calculated as $v = \sqrt{((pc1R1_{n+1} - pc1R1_n)^2 + (pc1R2_{n+1} - pc1R2_n)^2)}$, and velocity along a single dimension such as R1 simply as $v_{R1} = pc1R1_{n+1} - pc1R1_n$

Analysis of periodic and aperiodic spectrum components

To further investigate how power spectrum changes lead to the observed state-space effects, aperiodic and periodic components of the power spectrum were parametrized using the FOOOF algorithm (v. 1.0.0)

in Python 3.7 [32, 33]. First, average power spectra for each state were calculated from the sliding window FFT described earlier. One representative channel was analysed per rat and the same channel was used for the pre- and post-injection time points. For each spectrum, the frequency range from 1 to 45 Hz was used with the following algorithm settings: peak width limits: 0.5 and 12, maximum number of peaks: 6, minimum peak height: 0.2, peak threshold: 2.0, and aperiodic mode: knee. Aperiodic spectral components were modelled using the following aperiodic fit $AP(f) = 10^b * (1/(k + f^\chi))$ fit (AP) where f is frequency, b is offset, k is the knee parameter, and χ is the spectrum slope. The knee parameter represents the bending point where the aperiodic fit transitions from horizontal to negatively sloped. Knee frequency is dependent on the value of k and spectrum slope χ and was calculated as $k_{freq} = k^{(1/\chi)}$. Periodic components of the spectrum, representing putative oscillations, were modelled as Gaussian curves over and above the aperiodic background spectrum. These oscillations each have a center frequency (c), peak width (w), and center peak height (a), yielding the following for each oscillation frequency f $G(f) = a * \exp(-(f-c)^2/(2*w^2))$.

Cytokine quantification and histology

After recording, blood samples were collected and serum was separated by centrifugation at 1,000 × g for 10 min. Levels of IL-1β were quantified using ELISA kit according to manufacturer's protocol (RAB0277, Sigma).

After this, rats were killed using an overdose of sodium pentobarbital (50 mg/kg) and perfused transcardially with ringer solution followed by 4% paraformaldehyde in phosphate-buffered saline. Brains were collected and cut in 50µm thick coronal sections. Electrode placement was verified using Nissl staining. Electrode traces from electrodes outside of hippocampal CA3 were excluded from analysis.

Results

LPS increases serum IL-1β

To assess the effect of LPS on serum inflammatory cytokines, IL-1β levels were measured using ELISA. IL-1β concentrations in LPS-injected rats were at least 3 times higher than in saline-injected controls. (398 ± 32.24 pg/ml vs 122 ± 63.64 pg/ml, n = 6, independent sample t-test $t(10) = 3.88$, $p < 0.01$, Fig. S1).

LPS injection causes sleep state fragmentation

Under urethane anaesthesia rats showed two distinct patterns of brain activity: a NREM-like state that was dominated by high amplitude slow waves, and a REM-like state with low-amplitude, higher frequency activity (Fig. 1B-E). The states were long and stable at baseline and in saline-injected controls (Fig. 1B-D), but much shorter after LPS injection (Fig. 1E).

The total number of episodes per recording period was significantly affected by LPS injection (rmANOVA; group effect: $F(1, 10) = 5.14$, $p = 0.04$; time effect $F(1, 10) = 8.64$, $p = 0.01$; group*time interaction: $F(1, 10) = 8.55$, $p = 0.01$, Fig. 1F-G). Post-hoc analysis showed a significantly higher number of episodes after LPS

injection (87 ± 20 episodes) compared to before injection (24 ± 16 episodes). As a result, episode duration was also significantly altered (rmANOVA; group effect $F(1, 10) = 0.03$, $p = 0.85$; time effect: $F(1, 10) = 10.46$, $p < 0.01$; group*time interaction: $F(1, 10) = 5.58$, $p = 0.04$). Post-hoc analysis showed that episodes in the LPS group were significantly shorter after LPS injection (167 ± 36 s) than at baseline (694 ± 153 s).

Extensive sleep fragmentation after LPS injection was further apparent in episode length distribution (Fig. 2A). At baseline and after saline injection rats had few short episodes (20s -120s) and a relatively high number of long episodes (≥ 600 s). However, after LPS injection, brain activity patterns consisted of many short episodes and only a few long ones. These effects were present in both NREM and REM.

The relative number of short episodes in the recording period showed a significant time effect (rmANOVA; $F(1, 10) = 4.75$, $p = 0.05$) and group*time interaction ($F(1, 10) = 8.63$, $p = 0.01$), but no significant group effect ($F(1, 10) = 1.08$, $p = 0.32$). Post-hoc analysis showed an increase in the short episodes in the LPS group post injection (75 ± 4.6% of episodes) compared to pre-injection (44.1 ± 10.9% of episodes).

When quantified separately, relative amounts of short episodes in NREM were significantly higher in NREM after LPS injection, but not in REM. Short NREM episodes showed a significant time effect (rmANOVA; $F(1, 10) = 4.67$, $p = 0.05$) and a non-significant group effect ($F(1, 10) = 0.25$, $p = 0.62$). There was a significant effect of group*time interaction ($F(1, 10) = 19.78$, $p < 0.01$). Post-hoc analysis showed a significant increase in the percentage of short NREM episodes in the LPS group post injection (81.44 ± 4.58% of NREM episodes vs 46.59 ± 10.37% pre-injection, Fig. 2D). In REM, there was a significant group effect (rmANOVA; $F(1, 10) = 6.58$, $p = 0.02$) but a non-significant time effect ($F(1, 10) = 4.01$, $p = 0.07$) and group*time interaction ($F(1, 10) = 2.56$, $p = 0.14$). Post-hoc analysis showed a significant baseline difference between controls (70.12 ± 1.94%) and the LPS group (41.52 ± 11.88%) (Fig. 2C).

The percentage of long episodes in the recording period was also affected by LPS injection, but showed opposite effects to those observed for short episodes. The total percentage of all long episodes showed a significant effect of time ($F(1, 10) = 9.39$, $p = 0.01$) and group*time interaction ($F(1, 10) = 9.18$, $p = 0.01$), but no significant group effect ($F(1, 10) = 1.00$, $p = 0.34$). Post-hoc analysis showed a significant decrease in the percentage of long episodes in the LPS group post-injection (6.07 ± 1.55% of episodes) compared to pre-injection (42.20 ± 10.43% of episodes), although absolute numbers of long episodes are quite low.

Effects of LPS injection on NREM and REM states separately paralleled those found in the overall episode length distribution. The percentage of long NREM episodes showed a significant effect of time (rmANOVA; $F(1, 10) = 8.28$, $p = 0.01$) and group*time interaction ($F(1, 10) = 9.40$, $p = 0.01$). There was no significant group effect ($F(1, 10) = 0.79$, $p = 0.39$). Post-hoc analysis showed a decrease in the percentage of long NREM episodes after LPS injection (5.90 ± 1.55% of NREM episodes) compared to baseline (39.97 ± 10.48% of NREM episodes, Fig. 2F). Long REM episodes also showed a significant time effect (rmANOVA; $F(1, 10) = 9.78$, $p = 0.01$) and group*time interaction ($F(1, 10) = 8.39$, $p = 0.01$), but no significant group effect ($F(1, 10) = 0.89$, $p = 0.36$). Post-hoc analysis showed a significantly lower percentage of long REM episodes in the LPS group post-injection (6.51 ± 2.12% of REM episodes)

compared to pre-injection (44.16 ± 10.42% of REM episodes, Fig. 2E). These observed effects on episode number and duration point to fragmentation in both the REM- and NREM- state.

However, despite overall changes in episode length, the time spent in NREM (rmANOVA; time effect: $F(1, 10) = 0.002$, $p = 0.96$; group effect: $F(1, 10) = 0.77$, $p = 0.39$; group*time interaction : $F(1, 10) = 0.199$, $p = 0.66$) and in REM (rmANOVA; time effect: $F(1, 10) = 0.002$, $p = 0.96$, group effect: $F(1, 10) = 0.77$, $p = 0.39$; group*time interaction: $F(1, 10) = 0.199$, $p = 0.66$) was not significantly changed by LPS injection (Fig. 1H-I).

State fragmentation was also seen on the epoch-to-epoch level, where the probability of a state transition from one epoch to the next was similarly increased for NREM to REM transitions (rmANOVA; time effect: $F(1, 10) = 16.72$, $p < 0.01$; group effect: $F(1, 10) = 4.61$, $p = 0.06$; group*time interaction: $F(1, 10) = 10.53$, $p < 0.01$) and REM to NREM transitions (rmANOVA; time effect: $F(1, 10) = 16.12$, $p < 0.01$; group effect: $F(1, 10) = 4.77$, $p = 0.05$; group*time interaction: $F(1, 10) = 10.68$, $p < 0.01$). Post-hoc analysis showed a significantly higher probability of state transition from NREM to REM (0.17 ± 0.05% pre vs. 0.62 ± 0.10% post) and REM to NREM (0.17 ± 0.05% pre vs. 0.62 ± 0.09% post) in the LPS group post injection (Fig. S2). State transition probabilities remained at baseline levels in the CTRL group (NREM to REM: 0.22 ± 0.05% vs 0.27 ± 0.05%; REM to NREM: 0.27 ± 0.05% vs 0.27 ± 0.05%)

Although a higher number of state transitions was found after LPS injection, the characteristics of these transitions were not significantly different from those in controls or at baseline (Fig. S3). Thus, LPS injection leads to fragmentation of NREM and REM to a similar degree, without affecting time spent in either state, or the characteristics of transitions between the states.

LPS leads to increased spectral similarity between REM and NREM

State-space analysis of REM and NREM based on spectral power Ratio1 (R1, 1–9 Hz/1–2 Hz) and Ratio 2 (R2, 1–45 Hz/1–15 Hz) resulted in two distinct state clusters of epochs in the control group and LPS group at baseline and after injection (Fig. 3A-D).

After LPS injection (Fig. 3D), the location of the NREM and REM clusters within state-space shifted, resulting in a decreased inter-cluster distance. The magnitude and direction of the changes in cluster location after LPS injection and in controls is shown in Fig. 3E.

The centroid of REM cluster shifted significantly in LPS group (0.23 ± 0.05 a.u.) compared to control group (0.10 ± 0.03 a.u., $t(10) = 2.33$, $p = 0.04$, Fig. 3F). The direction of mean resultant vector is towards the origin for REM cluster (Fig. 3E). In case of NREM cluster, there was no significant difference between the cluster centroids of control (0.16 ± 0.04 a.u.) and LPS group (0.35 ± 0.06 a.u., $t(10) = 1.45$, $p = 0.17$). The mean resultant vector however is directed away from origin, towards the REM cluster (Fig. 3E).

As a result of the observed shifts in cluster medians, the total distance between the two clusters decreased (Fig. 3G). We calculated the total distance between REM and NREM clusters before and after

injection in control and LPS groups and observed a significant time effect ($F(1,10) = 26.47$, $p < 0.001$) and group*time interaction ($F(1,10) = 17.09$, $p < 0.01$). There was no group effect ($F(1, 10) = 0.3$, $p = 0.59$). Post-hoc analysis showed a significantly smaller distance between REM and NREM clusters in the LPS group post-injection (0.87 ± 0.19 a.u.) compared to baseline (1.30 ± 0.15 a.u.). The decreased inter-state cluster distance indicates increased spectral similarity between the states.

Spectral similarity in low frequency range

The decrease in distance between REM and NREM clusters could be the result of changes in R1, R2, or in both. By decomposing the total distance inter-cluster distance into R1 and R2 components, we determined which spectral range most affected post-LPS brain activity. Distance between the REM and NREM clusters was significantly decreased along R1 (rmANOVA; time effect $F(1, 10) = 39.26$, $p < 0.001$, group effect $F(1, 10) = 0.03$, $p = 0.84$, group*time interaction, $F(1, 10) = 27.55$, $p < 0.001$). Post-hoc analysis showed that the distance between clusters was significantly smaller in the LPS group post injection (0.69 ± 0.20 a.u.) compared to baseline (1.13 ± 0.14 a.u., Fig. S4A). By contrast, there was no significant change in the distance between the clusters along R2 (rmANOVA; time effect, $F(1, 10) = 2.85$, $p = 0.12$, group*time interaction, $F(1, 10) = 1.59$, $p = 0.23$, group effect, $F(1, 10) = 1.64$, $p = 0.22$, Fig. S4B).

Hence, LPS-mediated spectral similarity between REM and NREM is mostly the result of changes in the 1 to 9 Hz frequency range.

NREM contributes more to spectral similarity in lower frequencies than REM

After observing a reduced distance between REM and NREM clusters along R1, we investigated if this shift was state-specific or if both states contributed. In REM, we observed no significant changes in median R1 values (rmANOVA; time effect: $F(1, 10) = 3.16$, $p = 0.10$, group effect: $F(1, 10) = 0.0002$, $p = 0.98$, time*group interaction: $F(1, 10) = 4.31$, $p = 0.06$, Fig. S4C).

In NREM however, we found a significant time effect ($F(1, 10) = 15.02$, $p < 0.01$) and time*group interaction ($F(1, 10) = 7.27$, $p = 0.02$). There was no significant group effect ($F(1, 10) = 0.13$, $p = 0.72$). Post-hoc analysis showed a significant increase in R1 medians in the LPS group post-injection (0.61 ± 0.09 a.u.) compared to baseline (0.34 ± 0.09 a.u., Fig. S4D).

LPS causes instability within REM and NREM states

The observed state fragmentation and altered REM-NREM dynamics could be caused by to inflammation-related state instability. Here, we used within-state velocity, or the distance between subsequent epochs in state-space, as a measure of stability.

Velocities along R1 were not significantly affected by LPS injection in either REM (rmANOVA; time effect: $F(1,10) = 1.20$, $p = 0.29$; group effect: $F(1,10) = 0.80$, $p = 0.39$; time*group interaction: $F(1,10) = 0.01$, $p = 0.92$, Fig. S5A), or NREM (time effect: $F(1,10) = 0.92$, $p = 0.36$; group effect: $F(1,10) = 0.86$, $p = 0.37$; time*group interaction: $F(1,10) = 0.0005$, $p = 0.98$, Fig. S5B).

However, velocities along R2 were significantly increased in both REM and NREM after LPS injection. In REM, we observed a significant time*group interaction ($F(1,10) = 7.93$, $p = 0.01$) but no significant effect of group ($F(1,10) = 0.96$, $p = 0.34$) or time ($F(1,10) = 1.17$, $p = 0.30$) (Fig. S5C). Post-hoc analysis showed significantly higher velocities in the LPS group after injection compared to baseline (0.087 ± 0.03 a.u. vs. 0.074 ± 0.03 a.u.). The effects on R2 velocities in NREM were similar: there was a significant time*group interaction ($F(1,10) = 7.15$, $p = 0.02$), but no significant effect of group ($F(1,10) = 0.96$, $p = 0.34$) or time ($F(1,10) = 1.17$, $p = 0.30$, Fig. S5D). Post-hoc analysis showed no significant differences.

Effects of LPS on periodic and aperiodic power spectrum components

To investigate possible sources of the observed changes in R1, power spectra were analysed for representative channels. NREM spectra showed a marked reduction power below 3 Hz in LPS-injected rats, but not in controls (Fig. 4A). REM spectra showed the opposite effect: increased power in the < 3 Hz range, as well as a smaller increase in the 7–9 Hz range (Fig. 4B). Particularly in REM, these changes were quite variable. Power spectra of rats in the control group remained largely stable and at baseline levels.

The observed changes in spectral power ratios and spectral power distribution could be the result of alterations in EEG oscillations and in the background (aperiodic) components of the power spectrum. To better understand the observed changes in R1 in REM and NREM after LPS injection, aperiodic and periodic components of the power spectrum for each state were modelled using FOOOF in the LPS group. Overall model fits were good for NREM spectra ($R^2 = 0.995 \pm 0.002$, fit error = 0.031 ± 0.006) and REM spectra ($R^2 = 0.987 \pm 0.008$, fit error = 0.035 ± 0.007). Model fitting was not negatively affected by LPS injection (post-LPS fits in NREM: $R^2 = 0.996 \pm 0.002$, fit error = 0.029 ± 0.008, and REM: $R^2 = 0.985 \pm 0.011$, fit error = 0.035 ± 0.006).

Similar to non-anaesthetized recordings [34], REM spectra had overall slightly shallower slopes than the NREM spectra (pre-LPS REM vs. NREM exponents: 1.42 ± 0.28 vs. 1.95 ± 0.18; Fig. S6A-B). This was also the case after LPS injection (post-LPS REM vs. NREM exponents: 1.67 ± 0.22 vs. 2.09 ± 0.19; Fig. S6A-B)

The aperiodic components of the NREM spectra were not significantly affected by LPS injection (Fig. S6). Spectrum slopes remained stable at 107.5 ± 3.3% of pre-LPS slope values (Wilcoxon signed rank test, $W = 21$, $p = 0.09$ after Bonferroni correction, Fig. S6C), as did model offsets (102.15 ± 0.49%, $W = 21$, $p = 0.09$ after Bonferroni correction). Knee frequencies were more variable than the other parameters (pre-LPS: 1.83 ± 0.38 Hz, post-LPS: 2.68 ± 0.61 Hz) and showed a slight increase after LPS injection, but this effect was not significant (144.39 ± 11.36%, $W = 21$, $p = 0.09$ after Bonferroni correction, Fig. S6C).

Effects of LPS on aperiodic components in REM were similar to those observed in NREM (Fig. S6B). Like in the NREM spectra, REM slopes showed no significant changes after LPS injection (127.39 ± 15.09% of pre-LPS, $W = 16$, $p = 0.94$ after Bonferroni correction, Fig. S6D). NREM knee frequencies (pre-LPS: 5.37 ± 2.68 Hz, post-LPS: 5.49 ± 2.00 Hz, $W = 15$, $p = 1.31$ after Bonferroni correction, Fig. S6D) and spectrum

offsets were likewise not significantly affected (pre-LPS: 4.13 ± 3.44 a.u., post-LPS: 4.42 ± 0.35 a.u., W = 16, p = 0.94 after Bonferroni correction, Fig. S6D). They remained at 170.83 ± 77.38% and 107.63 ± 5.45% of baseline, respectively.

In pre-LPS recordings, NREM spectra showed one major periodic component: an oscillation in the delta frequency range with a mean center frequency of 1.56 ± 0.06 Hz and peak widths between 0.2 and 0.8 Hz (Fig. 4C-D). After LPS injection, center frequencies of this oscillation increased and peak widths became more variable (Fig. 4E-F). Overall, the main oscillatory component in NREM became faster and more variable after LPS injection. As such, the amount of spectral power in frequencies higher than 2 Hz increased, resulting in the observed shift in Ratio 1 in NREM.

REM spectra showed multiple oscillations: a delta-like oscillation with a peak frequency in the 1–2 Hz range, similar to the one found in NREM, and a second theta-like oscillation with a peak frequency around 5–6 Hz (Fig. 4G-H). These oscillations remained present after LPS injection, but more oscillations were found to have slower peak frequencies, and more oscillations had peak frequencies lower than 2 Hz. Additionally, REM peak widths became more variable, and overall peak heights tended to be slightly lower (Fig. 4I-J). This slowing of the oscillatory components in REM resulted in relatively more power in the 1–2 Hz range, while the power in frequencies over 2 Hz was decreased. This effect, opposite in direction to that found in the NREM spectrum, resulted in the decreased spectral distance between NREM and REM clusters observed in state-space.

Discussion

In the present study, we used the lipopolysaccharide model of sepsis in rats to characterize effects of severe generalized inflammation on brain oscillation state dynamics. We performed recordings under urethane anesthesia, which is known to largely spare the ongoing brain oscillations [28, 35]. Similar to previous results in septic awake behaving rats [18], we found profound fragmentation of the NREM-like and REM-like states in LPS-injected animals: episode lengths were shortened by approximately 75%. Additionally, the time spent in either state was not affected by LPS in our study, indicating that the observed fragmentation is unlikely to be the result of selective suppression of one of the states. Rather, it indicates that network state instability could be a result of the generalized inflammatory response.

Acute suppression of REM sleep is a common effect of inflammation [20] under non-anaesthetized conditions, in addition to fragmentation of the remaining NREM sleep and wakefulness. Although we do not find lower amounts of the REM-like urethane state in the current study, we do find increased switching between the slow-wave dominated NREM-like state and the higher frequency, low amplitude REM-like state. In the bistable state system under urethane, this resembles NREM fragmentation by wakefulness rather than by REM sleep in the non-anaesthetized system, where at least three stable vigilance states exist.

Sleep disturbances are a frequent complication of acute systemic inflammation in early- and developed-stage sepsis patients, and may persist in post-sepsis syndrome [11, 12, 36]. In the acute stage, state

fragmentation presents as many short sleep episodes that are widely distributed across the 24-hour period [18], indicating possible disturbances in both the homeostatic and circadian sleep regulatory systems: changes of central melatonin release rhythms [13], as well as circadian regulation of suprachiasmatic and HPA-axis activity [37–39]. Although the main molecular drivers of sleep homeostasis are not yet known, inflammation has been shown to affect expression of BDNF and adenosine 2A receptors [40–42], both of which have been linked to sleep homeostasis [20, 43]. Additionally, cytokine signaling plays an important role in regulating sleep pressure under normal circumstances [20].

LPS injection has been shown to cause degeneration of orexinergic neurons [44, 45]. It is therefore possible that the state instability observed in sepsis models (Baracchi et al., 2011, this paper) is in part related to the loss of these neurons [46, 47]. However, it is unclear how early this occurs during the disease progression, and therefore if orexin loss is sufficient to explain the occurrence of severe fragmentation as early as 25–30 minutes after LPS injection. Progressive loss of orexin during disease progression would likely also lead to cumulatively worse fragmentation, which is not in line with our observations.

To further investigate possible causes of state switching within the hippocampal network we used a power spectrum-based state-space approach. By plotting each epoch according to two spectral ratios and classifying as NREM or REM based on their position within the resulting state-space, we were able to study the relation between the states and the within-state dynamics. Similar state-space approaches have previously been used to study vigilance state dynamics in humans, mice, and rats [30, 31, 48–50].

Here, we found that the distance between NREM and REM clusters was reduced in septic animals. Similar decreases in inter-state distances accompanied by increased state fragmentation have been observed in narcolepsy patients and in orexin knockout mice, who have a narcolepsy-like phenotype [30], but so far not in sepsis patients or animal models. Reduced inter-state distances in state-space could therefore be a general characteristic of high state fragmentation, and may indicate altered attractor dynamics between stable states, facilitating state instability.

Decreased state-space distance between NREM and REM clusters is driven by opposing effects of LPS on these states within the lower frequency ratio R1. In NREM, this consisted of decreased delta power, as well as a shift towards faster oscillations within that frequency range. Decreases in NREM delta power have previously been described in sepsis in rats [18], although effects of lower doses of LPS on NREM delta power are less consistent [21, 25].

Increased delta and theta power, with high inter-individual variability, as well as a general slowing of oscillatory activity in the REM-like state under urethane is in line with slowing of EEG activity during awake, or wake-like states, described in sepsis patients. Relative increases in delta and theta power and reduced spectral peak frequencies were found in septic patients [51–54]. Increased slowing was associated with poor outcomes, including delirium [54] and death [55]. In animal models, increased wake delta power [56], slowed EEG [57], and reduced theta frequencies have been described [26]. Slowed EEG

may persist in former sepsis patients [19], but long term effects in animal models are less consistent [58–60].

It is not clear how much the previously described power spectrum changes are due to altered background spectrum or specific oscillatory activity, as the peak frequencies within spectral power bands were typically not analyzed. The occurrence of isolated delta and theta waves in the wake EEG of septic patients suggests that they are at least in part related to oscillations [14, 61, 62]. Unfortunately, most of the discussed papers limit their spectrum analysis to only one vigilance state, or in some cases to a single frequency band of interest. Where oscillatory activity is discussed, spectra were typically not decomposed into periodic and aperiodic components. Our results suggest, however, that oscillations are a main contributor to sepsis-related changes in power spectra in our model, while background shifts in E-I balance, as indicated by spectrum slope [63], were less prominent. Further studies that consider both sleep and wake states will be required to further elucidate NREM-REM interactions and the role of oscillatory and aperiodic brain activity in sepsis.

One hypothesized cause of increased state switching is state instability, as evidenced by high epoch-to-epoch variability within the states, resulting in high state-space velocity values. In line with this, we found higher within-state velocities in the higher frequency spectral ratio (R2) after LPS injection. Increased within-state velocities were previously observed in orexin knockout mice, but not in narcolepsy patients [30, 50]. In Parkinson's disease, which is characterized by low within-state velocities, sleep architecture is normal, but arousals in NREM were less common than in healthy controls [48]. Within Parkinson's patients, however, lower within-state velocities were associated with lower arousability. So, within-state velocities seem to be generally related to state stability, even if the instability doesn't always rise to the level of increased vigilance state changes. In septic rats, we found increased velocities in the higher frequency ratio, and not in the lower frequencies where we observed the largest overall shifts in cluster location. Changes in cortical higher frequency phenomena like spindles and HFOs signal NREM-REM transitions in normal sleep [64]. Increased variability in the higher frequencies, even outside of the transition periods themselves, may reflect increased state switching in our animals as well.

Despite the large degree of fragmentation after LPS injection, characteristics of the analyzed state transitions themselves remained normal. This in contrast to the narcolepsy phenotype, where fragmentation and high state velocities were associated with qualitative changes in state transitions [30]. This difference is likely a result of underlying pathophysiology, or of the more stereotypical brain activity characteristic of anaesthetized recordings. Alternatively, it is possible that the source of state switching is not within the hippocampal network itself, but rather results from disturbances in an upstream nucleus like lateral hypothalamus or locus coeruleus. A change in incoming transition signals combined with decreased inter-state distance could cause the hippocampal network to transition between states more often, but in an otherwise normal manner.

Given the role of sleep in maintaining a functional immune system and its association to memory consolidation, it's crucial to better understand sleep disturbances during sepsis. There is substantial proof

of memory impairments after sepsis, but the role of disturbed sleep remains to be fully explored. Remedying sleep fragmentation could be a potential treatment option for eventual recovery of memory impairments and cognitive function in sepsis survivors. Here, we aimed at getting a step closer to understanding these sleep state dynamics.

Conclusions

In summary, this study shows that the sleep-associated brain eeg states become highly instable during an acute stage of sepsis induced by LPS. Consequently, both REM- and NREM-like states became several times shorter than in control conditions, while their cumulative durations did not change. The eeg analysis showed opposing frequency shifts in slow oscillations (1–9 Hz) in REM and NREM. This resulted in increased spectral similarity between the states that might facilitate their frequent transitions and overall instability. This finding suggests a mechanism behind the severe fragmentation of sleep observed in patients with acute sepsis.

List Of Abbreviations

EEG
electroencephalogram
LFP
local field potential
LPS
lipopolysaccharide
NREM
non-rapid eye movement sleep
REM
rapid eye movement sleep
SABD
sepsis-associated brain dysfunction
rmANOVA
repeated measures analysis of variance

Declarations

Ethics approval and consent to participate

All protocols were approved by the Ethical Committee of the Ministry of Education, Youth and Sports of the Czech Republic (approval no. MSMT-12084/2019) according to the Guide for the Care and Use of Laboratory Animals (Protection of Animals from Cruelty Law Act No. 246/92, Czech Republic.).

Consent for publication

Not applicable

Availability of data and materials

The dataset used in this publication is available on request at *karel.jezek@lfp.cuni.cz*

Competing interests

The authors have no conflicts of interest to declare for this study.

Funding

The study was supported by Charles University projects START/MED/107 and Cooperatio / NEUR and by project CZ.02.1.01/0.0/0.0/16_019/0000787 „Fighting INfectious Diseases“, awarded by the MEYS CR and financed from EFRR.

Authors' contributions

AK, SL and KJ designed the study, AK recorded the data, AK and SL analysed the data, AK, SL and KJ wrote the manuscript. AK and SL contributed equally to the study.

Acknowledgements

We are very grateful to Lenka Sykorova and Stepan Kapl for technical support and Karel Blahna for his valuable inputs.

References

1. Annane D, Sharshar T. Cognitive decline after sepsis. Lancet Respir Med. 2015;3:61–9.
2. Rhee C, Dantes R, Epstein L, Murphy DJ, Seymour CW, Iwashyna TJ, et al. Incidence and Trends of Sepsis in US Hospitals Using Clinical vs Claims Data, 2009–2014. JAMA. 2017;318:1241–9.
3. Annane D, Sharshar T. Cognitive decline after sepsis. Lancet Respir Med. 2015;3:61–9.
4. Czempik PF, Pluta MP, Krzych ŁJ. Sepsis-Associated Brain Dysfunction: A Review of Current Literature. Int J Environ Res Public Health. 2020;17:5852.
5. Chavan SS, Huerta PT, Robbiati S, Valdes-Ferrer SI, Ochani M, Dancho M, et al. HMGB1 Mediates Cognitive Impairment in Sepsis Survivors. Mol Med. 2012;18:930–7.
6. Mostel Z, Perl A, Marck M, Mehdi SF, Lowell B, Bathija S, et al. Post-sepsis syndrome – an evolving entity that afflicts survivors of sepsis. Mol Med. 2020;26:6.
7. Pantzaris N-D, Platanaki C, Tsiotsios K, Koniari I, Velissaris D. The use of electroencephalography in patients with sepsis: A review of the literature. J Transl Intern Med. 2021;0:000010247820210007.
8. Yuan M. Effects of sepsis on hippocampal volume and memory function. World J Emerg Med. 2020;11:223.

9. Arwyn-Jones J, Brent AJ. Sepsis. Surg Oxf. 2019;37:1–8.
10. Freedman NS, Gazendam J, Levan L, Pack AI, Schwab RJ. Abnormal Sleep/Wake Cycles and the Effect of Environmental Noise on Sleep Disruption in the Intensive Care Unit. Am J Respir Crit Care Med. 2001;163:451–7.
11. Richards KC, Bairnsfather L. A description of night sleep patterns in the critical care unit. Heart Lung J Crit Care. 1988;17:35–42.
12. Weinhouse GL, Schwab RJ, Watson PL, Patil N, Vaccaro B, Pandharipande P, et al. Bench-to-bedside review: delirium in ICU patients - importance of sleep deprivation. Crit Care Lond Engl. 2009;13:234.
13. Bourne RS, Mills GH, Minelli C. Melatonin therapy to improve nocturnal sleep in critically ill patients: encouraging results from a small randomised controlled trial. Crit Care. 2008;12:R52.
14. Oddo M, Carrera E, Claassen J, Mayer SA, Hirsch LJ. Continuous electroencephalography in the medical intensive care unit*: Crit Care Med. 2009;37:2051–6.
15. Azabou E, Magalhaes E, Braconnier A, Yahiaoui L, Moneger G, Heming N, et al. Early Standard Electroencephalogram Abnormalities Predict Mortality in Septic Intensive Care Unit Patients. PloS One. 2015;10:e0139969.
16. Hosokawa K, Gaspard N, Su F, Oddo M, Vincent J-L, Taccone FS. Clinical neurophysiological assessment of sepsis-associated brain dysfunction: a systematic review. Crit Care Lond Engl. 2014;18:674.
17. Kinoshita H, Kushikata T, Takekawa D, Hirota K. Perioperative abnormal electroencephalography in a later-stage elderly with septic shock: a case report. JA Clin Rep. 2021;7:5.
18. Baracchi F, Ingiosi AM, Raymond RM, Opp MR. Sepsis-induced alterations in sleep of rats. Am J Physiol Regul Integr Comp Physiol. 2011;301:R1467-1478.
19. Semmler A, Frisch C, Debeir T, Ramanathan M, Okulla T, Klockgether T, et al. Long-term cognitive impairment, neuronal loss and reduced cortical cholinergic innervation after recovery from sepsis in a rodent model. Exp Neurol. 2007;204:733–40.
20. Opp MR. Cytokines and sleep. Sleep Med Rev. 2005;9:355–64.
21. Lancel M, Cronlein J, Muller-Preuss P, Holsboer F. Lipopolysaccharide increases EEG delta activity within non-REM sleep and disrupts sleep continuity in rats. Am J Physiol-Regul Integr Comp Physiol. 1995;268:R1310–8.
22. Borbély AA, Tobler I, Hanagasioglu M. Effect of sleep deprivation on sleep and EEG power spectra in the rat. Behav Brain Res. 1984;14:171–82.
23. Trachsel L, Tobler I, Borbely AA. Sleep regulation in rats: effects of sleep deprivation, light, and circadian phase. Am J Physiol-Regul Integr Comp Physiol. 1986;251:R1037–44.
24. Krueger JM, Kubillus S, Shoham S, Davenne D. Enhancement of slow-wave sleep by endotoxin and lipid A. Am J Physiol-Regul Integr Comp Physiol. 1986;251:R591–7.
25. Kapás L, Hansen MK, Chang H-Y, Krueger JM. Vagotomy attenuates but does not prevent the somnogenic and febrile effects of lipopolysaccharide in rats. Am J Physiol-Regul Integr Comp

Physiol. 1998;274:R406–11.
26. Mamad O, Islam MN, Cunningham C, Tsanov M. Differential response of hippocampal and prefrontal oscillations to systemic LPS application. Brain Res. 2018;1681:64–74.
27. Gofton TE, Young GB. Sepsis-associated encephalopathy. Nat Rev Neurol. 2012;8:557–66.
28. Clement EA, Richard A, Thwaites M, Ailon J, Peters S, Dickson CT. Cyclic and Sleep-Like Spontaneous Alternations of Brain State Under Urethane Anaesthesia. Greene E, editor. PLoS ONE. 2008;3:e2004.
29. Siegle JH, López AC, Patel YA, Abramov K, Ohayon S, Voigts J. Open Ephys: an open-source, plugin-based platform for multichannel electrophysiology. J Neural Eng. 2017;14:045003.
30. Diniz Behn CG, Klerman EB, Mochizuki T, Shih-Chieh L, E. Scammell T. Abnormal Sleep/Wake Dynamics in Orexin Knockout Mice. Sleep. 2010;33:297–306.
31. Gervasoni D, Lin S-C, Ribeiro S, Soares ES, Pantoja J, Nicolelis MAL. Global Forebrain Dynamics Predict Rat Behavioral States and Their Transitions. J Neurosci. Society for Neuroscience; 2004;24:11137–47.
32. Donoghue T, Haller M, Peterson EJ, Varma P, Sebastian P, Gao R, et al. Parameterizing neural power spectra into periodic and aperiodic components. Nat Neurosci. 2020;23:1655–65.
33. Haller M, Donoghue T, Peterson E, Varma P, Sebastian P, Gao R, et al. Parameterizing neural power spectra [Internet]. Neuroscience; 2018 Apr. Available from: http://biorxiv.org/lookup/doi/10.1101/299859
34. Leemburg S, Gao B, Cam E, Sarnthein J, Bassetti CL. Power spectrum slope is related to motor function after focal cerebral ischemia in the rat. Sleep [Internet]. 2018 [cited 2019 Aug 23];41. Available from: https://academic.oup.com/sleep/article/doi/10.1093/sleep/zsy132/5079131
35. Pagliardini S, Gosgnach S, Dickson CT. Spontaneous sleep-like brain state alternations and breathing characteristics in urethane anesthetized mice. PloS One. 2013;8:e70411.
36. Weinhouse GL, Schwab RJ. Sleep in the Critically ill Patient. Sleep. 2006;29:707–16.
37. Beynon AL, Coogan AN. Diurnal, age, and immune regulation of interleukin-1β and interleukin-1 type 1 receptor in the mouse suprachiasmatic nucleus. Chronobiol Int. 2010;27:1546–63.
38. Carlson DE, Chiu WC, Scalea TM. Cecal ligation and puncture in rats interrupts the circadian rhythms of corticosterone and adrenocortical responsiveness to adrenocorticotrophic hormone. Crit Care Med. 2006;34:1178–84.
39. Cavadini G, Petrzilka S, Kohler P, Jud C, Tobler I, Birchler T, et al. TNF-α suppresses the expression of clock genes by interfering with E-box-mediated transcription. Proc Natl Acad Sci U S A. 2007;104:12843–8.
40. Cui Y-H, Zhou S-F, Liu Y, Wang S, Li F, Dai R-P, et al. Injection of Anti-proBDNF Attenuates Hippocampal-Dependent Learning and Memory Dysfunction in Mice With Sepsis-Associated Encephalopathy. Front Neurosci. 2021;15:665757.
41. Ohta A, Sitkovsky M. Role of G-protein-coupled adenosine receptors in downregulation of inflammation and protection from tissue damage. Nature. 2001;414:916–20.

42. Pereira de Souza Goldim M, Della Giustina A, Mathias K, de Oliveira Junior A, Fileti ME, De Carli R, et al. Sickness Behavior Score Is Associated with Neuroinflammation and Late Behavioral Changes in Polymicrobial Sepsis Animal Model. Inflammation. 2020;43:1019–34.
43. Lanza G, DelRosso LM, Ferri R. Chapter 4 - Sleep and homeostatic control of plasticity. In: Quartarone A, Ghilardi MF, Boller F, editors. Handb Clin Neurol [Internet]. Elsevier; 2022 [cited 2022 Feb 1]. p. 53–72. Available from: https://www.sciencedirect.com/science/article/pii/B9780128194102000047
44. Perekrest SV, Abramova TV, Novikova NS, Loskutov YV, Rogers VJ, Korneva EA. Changes in immunoreactivity of orexin-A-positive neurons after intravenous lipopolysaccharide injection. Med Sci Monit Int Med J Exp Clin Res. 2008;14:BR127-133.
45. Perekrest SV, Novikova NS, Korneva EA. Brain Reactions Caused by Administration of Antigen. Adv Neuroimmune Biol. 2011;1:25–37.
46. Fronczek R, Schinkelshoek M, Shan L, Lammers GJ. Chapter 21 - The orexin/hypocretin system in neuropsychiatric disorders: Relation to signs and symptoms. In: Swaab DF, Kreier F, Lucassen PJ, Salehi A, Buijs RM, editors. Handb Clin Neurol [Internet]. Elsevier; 2021 [cited 2021 Dec 4]. p. 343–58. Available from: https://www.sciencedirect.com/science/article/pii/B9780128201077000215
47. Zeitzer JM, Buckmaster CL, Parker KJ, Hauck CM, Lyons DM, Mignot E. Circadian and Homeostatic Regulation of Hypocretin in a Primate Model: Implications for the Consolidation of Wakefulness. J Neurosci. 2003;23:3555–60.
48. Imbach LL, Sommerauer M, Poryazova R, Werth E, Valko PO, Scammell TE, et al. Bradysomnia in Parkinson's disease. Clin Neurophysiol. 2016;127:1403–9.
49. Imbach LL, Werth E, Kallweit U, Sarnthein J, Scammell TE, Baumann CR. Inter-Hemispheric Oscillations in Human Sleep. PLOS ONE. 2012;7:e48660.
50. Schoch SF, Werth E, Poryazova R, Scammell TE, Baumann CR, Imbach LL. Dysregulation of Sleep Behavioral States in Narcolepsy. Sleep [Internet]. 2017 [cited 2021 Oct 5];40. Available from: http://academic.oup.com/sleep/article/doi/10.1093/sleep/zsx170/4344838
51. Götz T, Baumbach P, Huonker R, Kranczioch C, Witte OW, Debener S, et al. Slowed peak resting frequency and MEG overactivation in survivors of severe sepsis and septic shock. Clin Neurophysiol Off J Int Fed Clin Neurophysiol. 2016;127:1247–53.
52. Rosengarten B, Krekel D, Kuhnert S, Schulz R. Early neurovascular uncoupling in the brain during community acquired pneumonia. Crit Care. 2012;16:R64.
53. Straver JS, Keunen RWM, Stam CJ, Tavy DLJ, de Ruiter GR, Smith SJ, et al. Nonlinear analysis of EEG in septic encephalopathy. Neurol Res. 1998;20:100–6.
54. Urdanibia-Centelles O, Nielsen RM, Rostrup E, Vedel-Larsen E, Thomsen K, Nikolic M, et al. Automatic continuous EEG signal analysis for diagnosis of delirium in patients with sepsis. Clin Neurophysiol. 2021;132:2075–82.
55. Yamanashi T, Marra PS, Crutchley KJ, Wahba NE, Malicoat JR, Sullivan EJ, et al. Mortality among patients with sepsis associated with a bispectral electroencephalography (BSEEG) score. Sci Rep. 2021;11:14211.

56. Kafa IM, Bakirci S, Uysal M, Kurt MA. Alterations in the brain electrical activity in a rat model of sepsis-associated encephalopathy. Brain Res. 2010;1354:217–26.
57. Kurita T, Takata K, Morita K, Uraoka M, Sato S. The Influence of Endotoxemia on the Electroencephalographic and Antinociceptive Effects of Isoflurane in a Swine Model. Anesth Analg. 2010;110:83–8.
58. Gao R, Ji M-H, Gao D-P, Yang R-H, Zhang S-G, Yang J-J, et al. Neuroinflammation-Induced Downregulation of Hippocampacal Neuregulin 1-ErbB4 Signaling in the Parvalbumin Interneurons Might Contribute to Cognitive Impairment in a Mouse Model of Sepsis-Associated Encephalopathy. Inflammation. 2017;40:387–400.
59. Ji M, Li S, Zhang L, Gao Y, Zeng Q, Mao M, et al. Sepsis induced cognitive impairments by disrupting hippocampal parvalbumin interneuron-mediated inhibitory network via a D4-receptor mechanism. Aging. 2020;12:2471–84.
60. Wang Y, Wei H, Tong J, Ji M, Yang J. pSynGAP1 disturbance-mediated hippocampal oscillation network impairment might contribute to long-term neurobehavioral abnormities in sepsis survivors. Aging [Internet]. 2020 [cited 2021 Dec 7]; Available from: http://www.aging-us.com/article/104080/text
61. Bolton CF. Electrophysiologic studies of critically ill patients. Muscle Nerve. 1987;10:129–35.
62. Kaplan PW, Rossetti AO. EEG Patterns and Imaging Correlations in Encephalopathy: Encephalopathy Part II. J Clin Neurophysiol. 2011;28:19.
63. Gao R, Peterson EJ, Voytek B. Inferring synaptic excitation/inhibition balance from field potentials. NeuroImage. 2017;158:70–8.
64. Sánchez-López A, Silva-Pérez M, Escudero M. Temporal dynamics of the transition period between nonrapid eye movement and rapid eye movement sleep in the rat. Sleep [Internet]. 2018 [cited 2022 Jan 31];41. Available from: https://academic.oup.com/sleep/article/doi/10.1093/sleep/zsy121/5042786

Figures

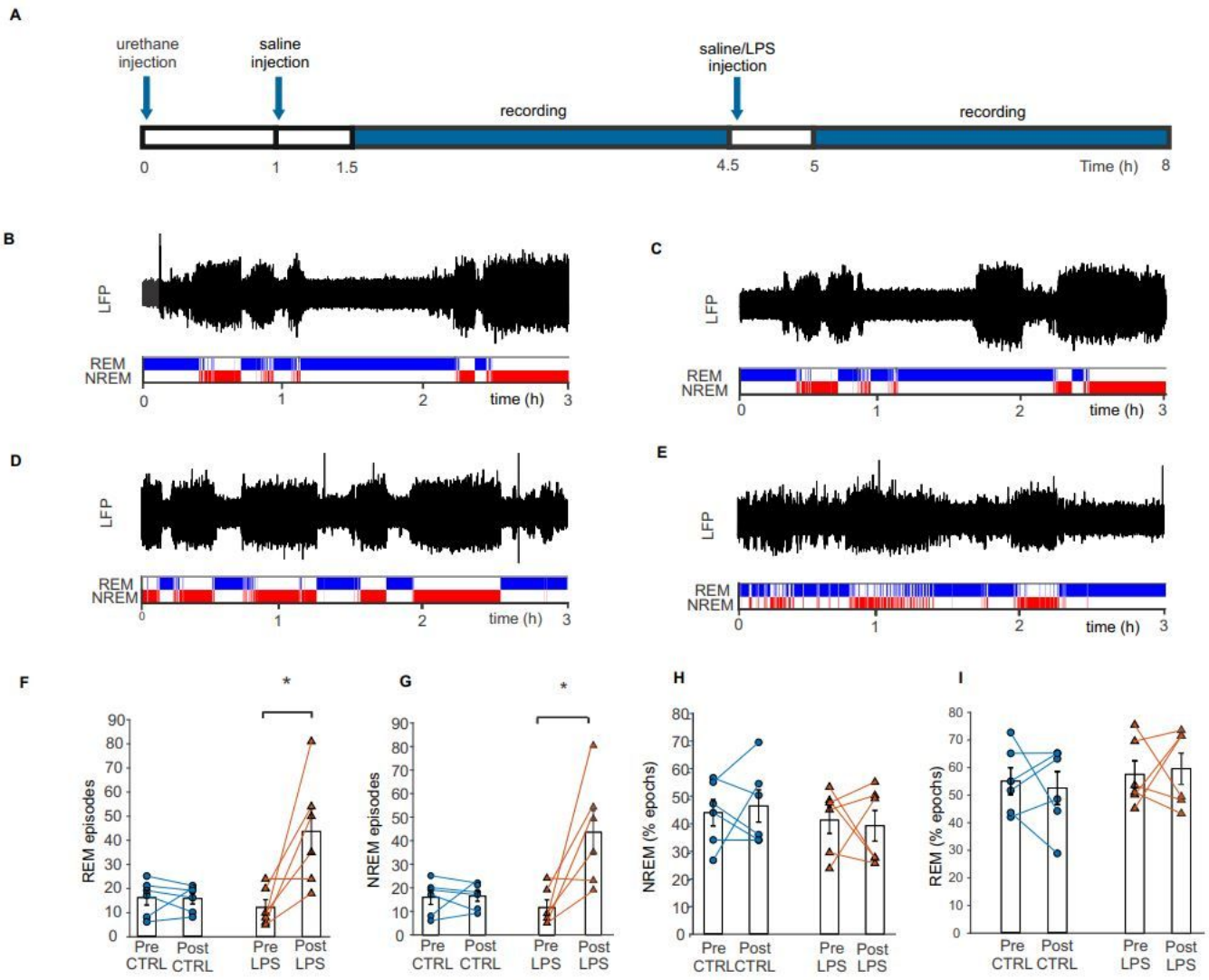

Figure 1

LPS causes sleep state fragmentation in rats without affecting the total time spent in either state.

A. Experimental design- rats in urethane anesthesia were injected with saline and baseline LFP was recorded for 3-hours, followed by a dose of LPS (LPS, n=6) or saline (CTRL, n=6) and a 3-hour LFP test recording.

B-E. Representative traces and hypnograms showing the REM-like state in blue, NREM in red. Sleep states were long and stable before (B) or after saline injection (C) in CTRL group and before the LPS injection (D) in the LPS group. After LPS injection (E), sleep states were heavily fragmented.

F. Amount of REM episodes before and after the treatment. Each data point shows the number of REM episodes in individual CTRL and LPS animals pre and post injection, respectively (CTRL, n = 6; LPS, n = 6).

G. Number of NREM episodes in CTRL and LPS animals pre and post injection, respectively.

H. Total time spent in REM as percentage of recording time in CTRL and LPS animals pre and post injection, respectively.

I. Total time spent in NREM as percentage of recording time in CTRL and LPS animals pre and post injection, respectively. Bar graphs show mean ± s.e.m. *p < 0.05.

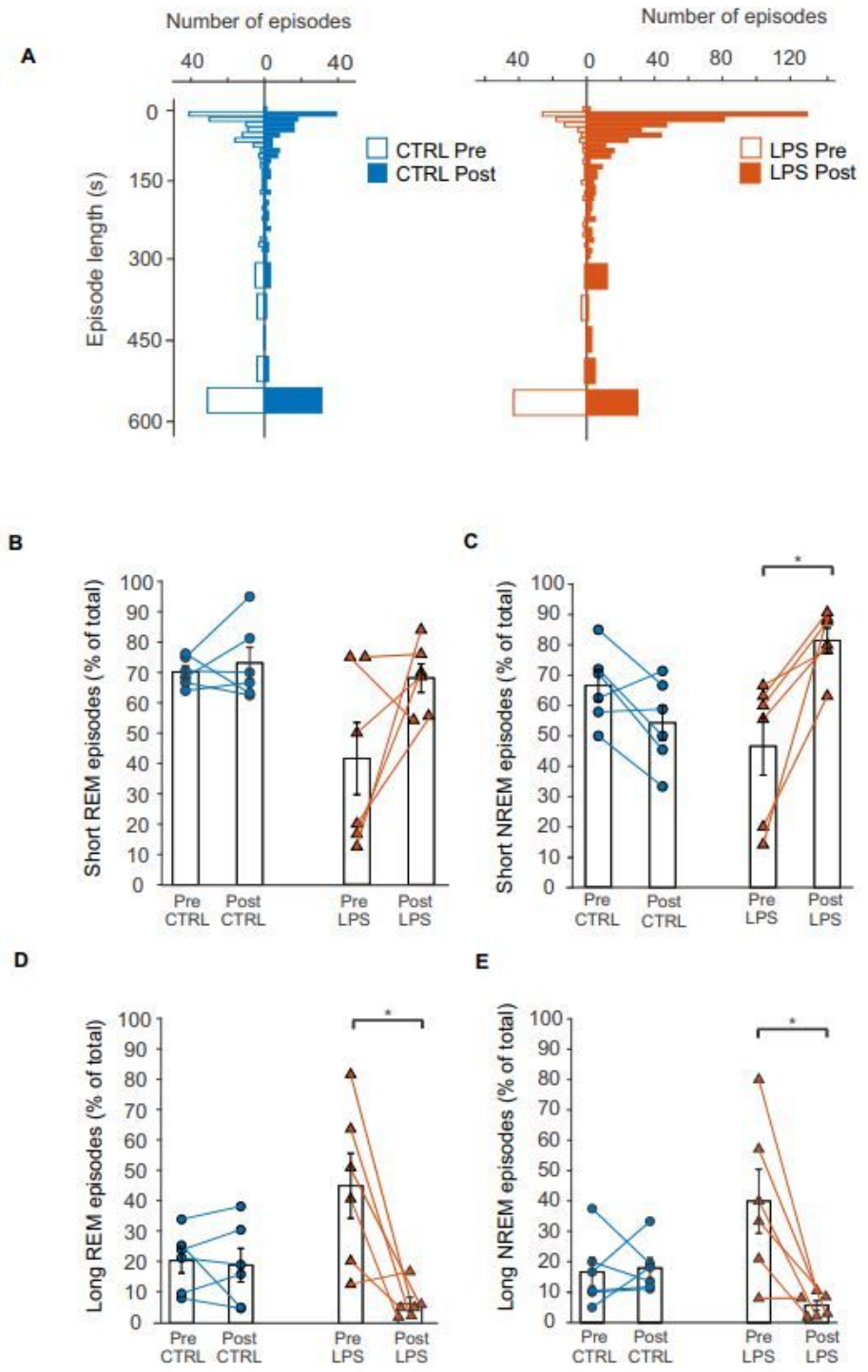

Figure 2

LPS leads to an increase in short and to a decrease in long sleep state episodes.

A. Histograms depicting the overall distribution of episode lengths in CTRL (left) and LPS rats (right), pre and post injection. Each bar in the histogram represents the number of episodes per 10- or 50-s bin.

B-C. Proportions of short (20s-120s) episodes of REM (B) or NREM (C) in CTRL and LPS rats, pre and post injection, respectively (CTRL, n = 6; LPS, n = 6) in the recording.

D-E. Proportions of long (≥600s) episodes of REM (D) or NREM (E) in CTRL and LPS rats, pre and post injection, respectively. Bar graphs show mean ± s.e.m. *p < 0.05.

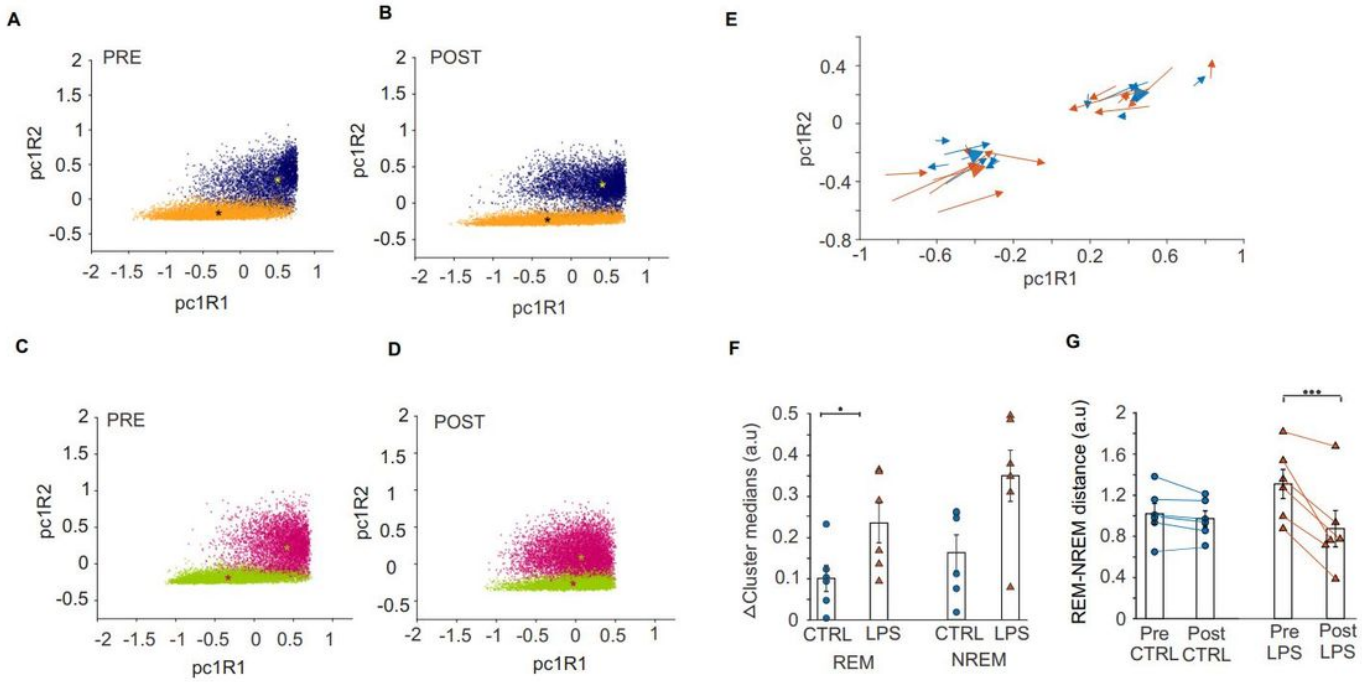

Figure 3

LPS leads to reduced cluster distance between REM and NREM oscillatory states.

A-D. Scatter plots showing REM and NREM epochs in 2-D state space in CTRL (A, B) and LPS (C, D) groups, pre and post injection, respectively. The asterisk marks the cluster median.

E. Quiver plot showing the directional shift of the REM and NREM cluster medians before and after injection in CTRL (blue) and LPS animals (orange). The starting point of each arrow shows cluster medians before the injection, and the arrow head the medians after the injection.

F. Each data point represents the shift of REM (left) or NREM (right) clusters after the treatment in individual CTRL or LPS animals, respectively.

G. The distance between REM and NREM clusters in CTRL or LPS animals pre and post injection. Bar graphs show mean ± SEM. *p<0.05; ***p<0.001.

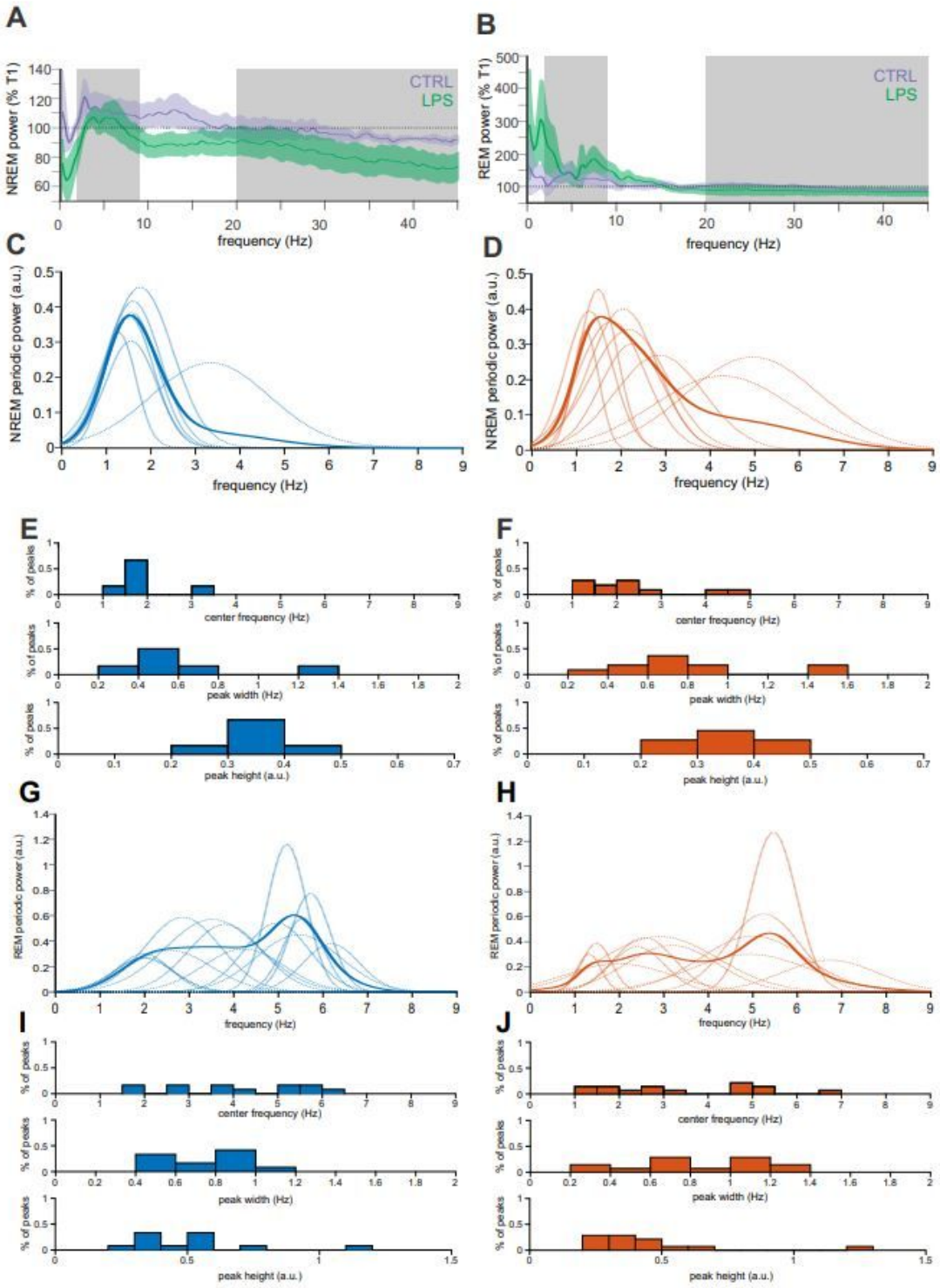

Figure 4

LPS-related changes in NREM and REM power spectra.

A. NREM power spectra of control (purple) and LPS-injected (green) rats as percentage of pre-injection baseline (T1). Grey areas indicate limits of the spectral ratios used for state-space analysis.

B. REM power spectra of control (purple) and LPS-injected (green) rats as percentage of pre-injection baseline (T1). Grey areas as in (A).

C-D. NREM oscillations in the 1-9 Hz frequency range prior (C) and after (D) the LPS injection. Dotted lines show individual values solid line shows the mean oscillatory power.

E-F. Distribution of NREM oscillation characteristics before (E) and after (F) the LPS injection.

G-H. REM oscillations in the 1-9 Hz frequency range prior (G) and after (H) the LPS injection. Lines as in (C).

I-J. Distribution of REM oscillation characteristics before (I) and after (J) the LPS injection.

Supplementary Files

This is a list of supplementary files associated with this preprint. Click to download.

- SupplementalFiguresKalaetal.pdf